Nano Energy 72 (2020) 104666

Contents lists available at ScienceDirect

Nano Energy

journal homepage: http://www.elsevier.com/locate/nanoen

Full paper

Energy density-enhancement mechanism and design principles for heteroatom-doped carbon supercapacitors

Yong Gao [a], Jing Zhang [a], Xian Luo [a], Yiyang Wan [b], Zhenghang Zhao [b], Xiao Han [a], Zhenhai Xia [b,*]

[a] State Key Laboratory of Solidification Processing, School of Materials Science and Engineering, Northwestern Polytechnical University, Xi'an, Shaanxi, 710072, China
[b] Department of Materials Science and Engineering, Department of Chemistry, University of North Texas, Denton, TX, 76203, USA

ARTICLE INFO

Keywords:
Supercapacitor
Carbon nanomaterials
Heteroatom-doped graphene
Energy storage
First principles calculation

ABSTRACT

Carbon-based pseudo-supercapacitors are one of the most promising electrical energy storage devices with high power density and long cycle life which is strongly desired for electric vehicles but their capacitance needs to be improved. Here, a new approach and design principle to enhance the energy density have been developed with the density functional theory methods. The results reveal that compared with pure carbon, the energy density could be enhanced significantly via heteroatom-doping. An intrinsic descriptor is discovered to establish a volcano-shaped relationship that correlates the capacitance with the heteroatom-doping structures of carbon nanomaterials, from which the best electrode structures are identified, which are in good agreement with the experimental results. Th strategies for further enhancing energy densities are proposed for rational design and fabrication of high-energy-density supercapacitors.

1. Introduction

Supercapacitors are one of the most effective electric energy storage devices in terms of their long cycle life (one million) and high power density. In particular, the power density of the supercapacitors is 100 times greater than conventional batteries. However, the energy density is approximately 10% of the conventional batteries. Thus, increasing the energy density of the supercapacitors holds promise for solving critical problems in energy storage technologies for various applications such as electric vehicles [1–5].

In supercapacitors electric energy is stored by the electrostatic adsorption of charges (i.e., electric double-layer capacitor (EDLC)) and/or the chemisorption of charges on the surface of the electrodes (so-called pseudocapacitor). The electrode materials therefore play a key role in determining the energy density, power density and cycle life. Generally, the most effective way to enhance the capacitance of the capacitors is to modulate the surface polarity and electronic property of electrode materials to deliver extra pseudocapacitance from the robust faradic reactions (commonly 10–100 times larger than the original EDLC). Various materials have been investigated for designing better electrode materials, including nanoporous carbon, conductive polymer, metal-organic frameworks (MOF), two-dimensional transition-metal dichalcogenides (2D TMDs), titanium carbide MXenes, metal oxides, metal nitrides, and metal carbides [6–12]. Carbon nanomaterials, including carbon nanotubes, carbon nanofibers, and graphene, are one of the most promising electrode materials owning to their unique structures, excellent electrical, mechanical, and thermal properties, large specific surface area, and chemical inertness in acidic and alkaline environments. Recently extensive research has been carried out to exploit the carbon nanomaterials for energy storage applications such as fuel cells [13], metal-air batteries [14], water splitting and supercapacitors [15]. Carbon nanomaterials used as supercapacitor electrodes include two-dimensional layered graphene without restacking [16], three-dimensional porous activated carbon [17], onion-like carbon spheres [18], hybrid configuration though grafting carbon nanotubes to graphene sheets [19]. In particular, heteroatom-doping technique has been applied to improve the energy storage capacity of the carbon electrodes in supercapacitors. It has been demonstrated that heteroatom dopants such as nitrogen, boron and phosphorus, can significantly enhance both energy and power densities of graphene-based pseudocapacitors [20–22]. The doping with certain elements can even expand the voltage window of aqueous electrolytes, which further enhances the energy density [23].

Although the superior energy storage capabilities of heteroatom-

* Corresponding author.
E-mail address: Zhenhai.xia@unt.edu (Z. Xia).

https://doi.org/10.1016/j.nanoen.2020.104666
Received 17 November 2019; Received in revised form 28 February 2020; Accepted 29 February 2020
Available online 5 March 2020

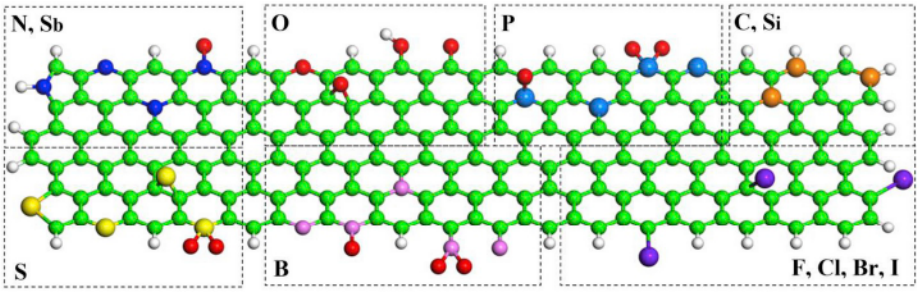

Fig. 1. Schematics of the p-element doping configurations and molecular models for graphene sheet and nanoribbons. Summary of the heteroatom doping modes: (top row, from left to right) pr-N(Sb), py-N(Sb), g-N(Sb), N(Sb)–O, py-O, C–O–C, C–OH, CO, 3C–P–O, P–3C, 2C –P–2O, P–2C, g-C(Si), z-C(Si) and a-C(Si); (bottom row, from left to right) th-S, py-S, C-S-C, 2C-S-2O, B–2C, 2C-B-O, B–3C, C-B-2O, BC, z-(F, Cl, Br, and I), g-(F, Cl, Br, and I) and a-(F, Cl, Br, and I); Green, blue, red, white, cadetblue , orange , yellow, orchid, and blue violet represent C, N(Sb), O , H, P, C(Si), S, B, and F (Cl, Br, and I) atoms, respectively.

doped carbon nanomaterials for supercapacitors have been demonstrated, trial-and-error approaches are still used to date for the development of high-performance supercapacitors. To rationally design effective electrode materials, it is necessary to correlate the doping structures to the capacitance of carbon-based electrodes. Some work has been done by using the first-principles calculations to understand the energy storage mechanisms and to estimate charge storage ability of heteroatom-doped carbon electrodes [24,25]. For the entire family of metal-free carbon-based electrodes, however, there lacks design principles or intrinsic descriptors that govern charge storage activities. Herein, we investigate charge storage performance of the graphene structures doped with p-block elements in the periodic table. The specific capacitance C, energy density E and power density P are correlated with the heteroatom-doping structures of carbon nanomaterials by an intrinsic descriptor that can be used for screening the best electrode materials. The predictions are consistent with the experimental results. The design principles for enhancing both energy and power densities of carbon-based pseudocapacitors are established based on the results. The results provide a theoretical base for searching for the desired carbon-based electrode materials for high-performance pseudocapacitors.

2. Results and discussion

2.1. Charge storage mechanism of heteroatom-doped carbon

To understand charging and discharging mechanisms of heteroatom-doped carbon nanomaterials, we created a series of the graphene (G) structures doped with p-block elements (X) in the periodic table (X = N, Sb, B, P, F, Cl, Br, I, S, O and Si) (Fig. 1, and Fig. S1). Using the first principles calculation, the elementary charging and discharging steps on possible sites of the materials were simulated by introducing protons near the sites. During the charging, an external electrical potential U_a is applied to drive electrons to the charge storage sites on the electrode surface while protons in acid electrolyte are adsorbed physically or chemically on the sites. This charging process can occur spontaneously, depending on the change in the Gibbs free energy of adsorption ($\Delta G_{H^*}(U)$), where U is the applied potential. If $\Delta G_{H^*}(U) > 0$, protons may adsorb physically to the sites to form electric double-layers (EDLC). Otherwise, protons are chemisorbed on the sites by combining with the electrons (pseudocapacitor). In discharging, the physically adsorbed protons would enter the electrolyte by releasing an electron. For the chemisorbed protons, discharging occurs when they desorb to the electrolyte due to electrons leaving from electrode surface (reverse Volmer reaction) as a result of the work done by supercapacitors though external circuits. Thus, the charging/discharging processes of pseudocapacitors can be described by

$$H^+ + e^- + * \underset{\text{Discharging}}{\overset{\text{Charging}}{\rightleftharpoons}} H^* \quad (1)$$

where * refers to a site of heteroatom-doped graphene (X-G). Therefore, the possible sites for charge storage can be identified by evaluating ΔG_{H^*} (Figs. S2 and S3).

Using density functional theory (DFT) methods, we have calculated ΔG_{H^*} for all the sites of the possible X-G structures under an applied potential of $U_a = 0$. The typical distributions of ΔG_{H^*} on the adsorption sites of heteroatom-doped structures are shown in Fig. 2a, b and c. Basically, the ΔG_{H^*} distributes uniformly on basal plane of the graphene while in the area near its edge and dopants (Fig. 2a, b and c), it becomes relatively low or largely disturbed. These results indicate that there are edge and doping effects, which largely change the landscape of the hydrogen adsorption. The distribution range of ΔG_{H^*} for doped and undoped graphene structures are summarized in Fig. 2d. The doped graphene has a relatively large range of ΔG_{H^*} compared with pristine one.

According to pseudocapacitive mechanism, the ability to store electrical charges in the supercapacitors depends on the chemisorption of protons on the effective sites of the electrode materials under certain applied electrical potential U_a. However, during the charging the external potential cannot exceed the decomposition voltage of electrolytes ($U_d = 1.23$ V for aqueous electrolytes). On the other hand, during the discharging the adsorption energy must be larger than zero ($\Delta G_{H^*} > 0$) such that the chemisorbed protons can be released from the sites during discharging since the proton chemisorption is exothermic for those sites with $\Delta G_{H^*} < 0$, and will not desorb spontaneously from the sites during the discharging. These two constraints draw a window of effective charge storage with two bound limits, as shown in Fig. 2d. While the upper bound is defined by the decomposition voltage of electrolytes, $U_d = 1.23$ V, the lower bound is described by the Gibbs free energy of adsorption ($\Delta G_{H^*} = 0$). Therefore, ΔG_{H^*} can be used as an indicator to identify possible charge storage sites of the X-G. The active sites for charge storage are defined in the range of $0 < \Delta G_{H^*} < U_d$; otherwise, it is an inactive one. The smaller the ΔG_{H^*}, the lower the external potential applied to store charges. This provides an approach to accurately estimate the active area for charge storage in electrode materials. Such an approach is different from those that solely consider the number of ions such as H^+, Na^+ and K^+ chemisorption on electrode surfaces as a criterion for charge storage capacity [24], which may overestimate the charge storage capacity due to the existence of inactive sites.

On the basis of above definition of the active sites for energy storage on heteroatom-doped carbon electrode, the capacitance of unit charge storage site $C_{0/site}$ and the area specific capacitance C_A (Support Information), can be correlated approximately to the external electric potential U and the minimum positive free energy of hydrogen adsorption, $\Delta G_{H^*}^{min}$, in the range of $0 < \Delta G_{H^*}^{min} < eU < \Delta G_{H^*}^{max}$ by

$$C_{0/site} = \frac{\frac{1}{2}e^2\left(\frac{eU-\Delta G_{H^*}^{min}}{\Delta G_{H^*}^{max}-\Delta G_{H^*}^{min}}\right)^2}{\frac{eUk_BT}{eU-\Delta G_{H^*}^{min}} ln\left[\frac{1}{2}\left(1+e^{\frac{eU-\Delta G_{H^*}^{min}}{k_BT}}\right)\right]} \quad (2a)$$

where $C_{0/site}$ is the capacitance per unit site (unit, e V^{-1}), and U is the

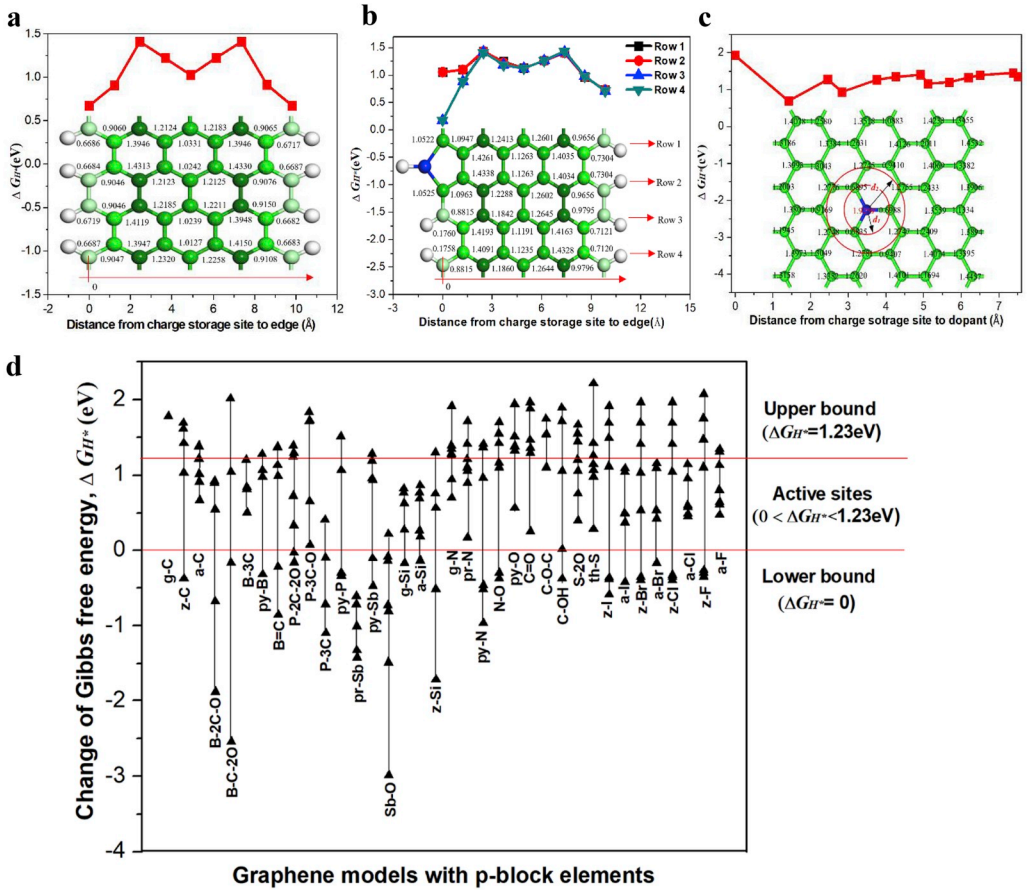

Fig. 2. Distribution of change of Gibbs free energy (ΔG_{H^*}) and bar graph of computed Gibbs free energy ΔG_{H^*} at $U = 0$. Distribution of change of Gibbs free energy (ΔG_{H^*}) for **a**. armchair graphene, **b**. pr-N graphene nanoribbons and **c**. g-N graphene nanosheet. **d**. bar graph of computed Gibbs free energy ΔG_{H^*} at $U = 0$.

external electric potential.

For $eU \geq \Delta G_{H^*}^{max}$, the specific capacitance $C_{0/\text{site}}$ (Support Information) can also be given by

$$C_{0/site} = \frac{C_T}{M} = \frac{e^2\left(\frac{1}{N}\sum_{i=0}^{N}\theta_i\right)^2}{2E_{0/site}} = \frac{e^2}{\Delta G_{H^*}^{min} + \Delta G_{H^*}^{max}} \quad (2b)$$

According Equation (2a), the capacitance increases with decreasing the $\Delta G_{H^*}^{min}$, while it increases continuously with increasing U, as shown in Fig. 3a and b. This is mainly due to more active sites triggered by higher external electric potential U or lower adsorption energy $\Delta G_{H^*}^{min}$ in the range of $0 < \Delta G_{H^*}^{min} < eU < \Delta G_{H^*}^{max}$. However, for $eU > \Delta G_{H^*}^{max}$ all the active sites are occupied, and the capacitors achieve its upper limit of capacitance. With decreasing the adsorption energy $\Delta G_{H^*}^{min}$, the specific capacitance $C_{0/site}$ increases. Therefore, doping enhances specific capacitance effectively by means of reducing the minimum free energy of hydrogen adsorption or increasing the applied potentials. From above discussion, an effective strategy to enhance the charge storage capability

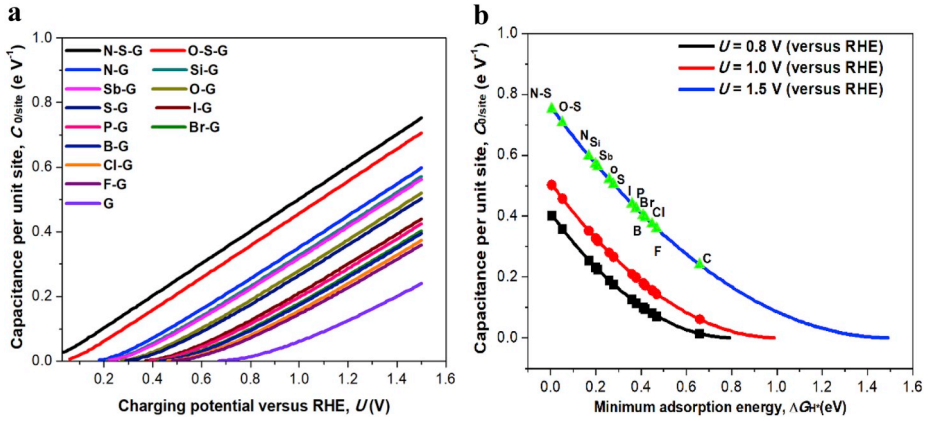

Fig. 3. Capacitance per unit site versus **a**. charging potential U (versus RHE) and **b.** minimum adsorption energy $\Delta G_{H^*}^{min}$ for mono-and multi-doped graphene models with different $\Delta G_{H^*}^{min}$ in the range of $0 < \Delta G_{H^*}^{min} < eU < \Delta G_{H^*}^{max}$.

is to move ΔG_{H^*} into the active window defined by the bound limits. As shown in Fig. 2d, graphene basal plane does not have charge storage ability at all by pseudocapacitive mechanism, which was demonstrated by previous study [26], while the ΔG_{H^*} for both zigzag and armchair carbon nanoribbons partially fallen into the window, indicating a limiting charge storage capability. In contrast, doping with p-block elements lowers ΔG_{H^*}, which significantly reduces the energy barriers for protons chemisorption on the active sites of the doped graphene, and thus promotes proton adsorption and therefore energy storage.

2.2. Design principle of heteroatom-doped carbon-based electrode materials

It is of interest to develop a computational approach that has predictive power for rational design of the best doping structures for energy storage. To achieve this goal, it is necessary to establish the design principles or intrinsic descriptors that correlate the energy storage capacity with the doping structures. We found that the energy storage properties of the materials can be well described by the descriptor Ø [13].

$$\text{Ø} = \frac{E_X A_X}{E_C A_C} \tag{3}$$

where E_X and A_X are electronegativity and electron affinity of dopants in graphene substrate, respectively, and E_C and A_C are electronegativity and electron affinity of carbon element, respectively.

Fig. 4a show the lowest values of the Gibbs free energy of adsorption (ΔG_{H^*}) on heteroatom-doped graphene as a function of descriptor Ø. ΔG_{H^*} is correlated with the descriptor to form a inverted volcano relationship with N-doping at the summit of the volcano, which predicts that N dopant is the best one among the dopants tested in this work. The energy density ($E_{0/site}$) or capacitance ($C_{0/site}$) also has the similar volcano relationship with the descriptor (Fig. S4). Such a descriptor has a predictive power for screening the X-G for electrode materials.

To verify the proposed descriptor, the specific capacitances of the X-G materials, measured experimentally were cited from the literatures [27–32]. To reliably compare the measured specific capacitances with our predictions, firstly, all the experimental data cited in this work were measured in the same acid electrolyte (H_2SO_4), and the specific surface area is accounted for in the calculations of specific capacitances (capacitance per unit area). The specific capacitances were then normalized by the specific capacitance of undoped graphene electrode, measured under the same condition in the same experiment. Although morphology of the materials and dopant content could also affect the specific capacitances, since only graphene were selected, their morphology and dopant content are similar and comparable. To further minimize the possible morphology/dopant content effects, we have averaged the data that were carefully selected from the literatures. The measured capacitance is plotted as a function of the descriptor in Fig. 4b.

Theoretical computing specific capacitance of the X-G were also normalized by that of undoped graphene, and also plotted in Fig. 4b as a function of the descriptor for the X-G. Clearly, the experimental results show a volcano relationship with nitrogen sitting on its top, which agrees well with the predictions. Thus, the descriptor provides a theoretical tool to predict the energy storage capacity of the X-G, from which the best electrode materials could be selected.

The predictive power of the descriptor Φ originates from its intrinsic physical meaning that correlates the properties to the structure of active sites. According to the definition of Pauling and Mulliken, the electrode chemical potential μ is related to the electronegativity by $\mu \approx -\chi_M$, where χ_M is the Pauling and Mulliken electronegativity. In charging process, the total energy of electrode resulting from adding an electron will also increase, which is given by $eU = \mu(N+1) - \mu(N)$, where $\mu(N)$ and $\mu(N+1)$ represent the chemical potential of doping graphene with N-electrons and (N+1)-electrons resulting from external power supply at ground state. Finally, at ground state, capacitance can be related to electronegativity, or our descriptor by $C_{0/site} = \frac{e^2}{\chi_M(N) - \chi_M(N+1)}$. Therefore, the capacitance is directly related to the electronegativity.

2.3. Further improvement of electrodes and theoretical limit of doping theory

According to the predictions of the volcano relationship, there is still a large room for us to improve the capacitance towards the ideal charge storage capacity (Fig. 4a). Here, a strategy of co-doping is used to further increase the charge storage capacity. Since N is the best dopant among the p-orbital elements, it is selected to combine with the second best dopant S to form N, S co-doped graphene structures (Fig. S5). These co-doped structures were examined to determine the active sites with the desired $\Delta G_{H^*}^{min}$ using the same method as the single-element doping. As expected, $\Delta G_{H^*}^{min}$ can be further reduced by co-doping (Fig. 5a and b), and the capacitance of the capacitors can be pushed to its limitation (Fig. 5c and d). These predictions are consistent with the experimental results [33]. In order to compare the difference between co-doped structures, we selected two second best dopants relative to dopant N to form O, S co-doped graphene structures (Fig. S6). The results showed that O, S co-doped carbon electrode is better than single N-doping, but less active than the N, S co-doping. We have quantitatively estimated the theoretical capacitance based on the adsorption mechanism of on graphene substrate. The theoretical maximum capacitance of the N, S co-doping electrodes with H_2SO_4 electrolyte can achieve 606 μC cm^{-2}. The high charge storage capacity of the co-doped carbon electrodes can be attributed to the synergistic effect between the dopants. This synergetic effect originates from the valence electron interactions between dopants [34].

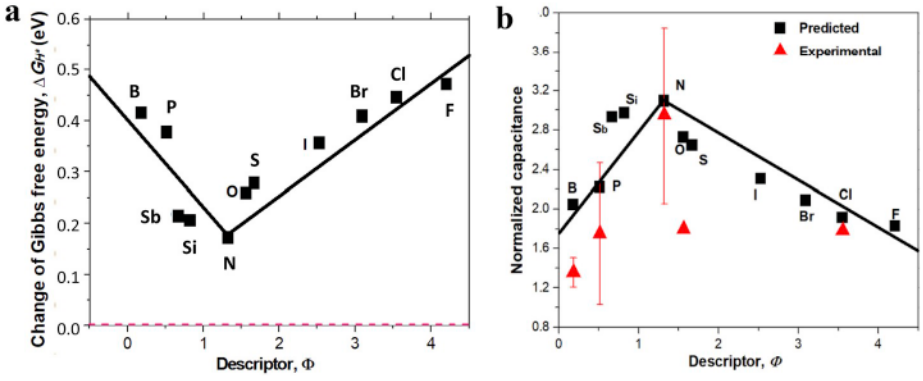

Fig. 4. The adsorption energy and capacitance for X-doped graphene structures versus descriptor Ø. a, the minimum Gibbs free energy of adsorption versus descriptor. **b**, Measured specific capacitance from electrochemical measurements, normalized by undoped pure carbon-based electrode in H_2SO_4 electrolyte under the same condition in the same experiment, and the predictions [32–36]. The predicted specific capacitance, normalized by undoped graphene, is also plotted against the descriptor.

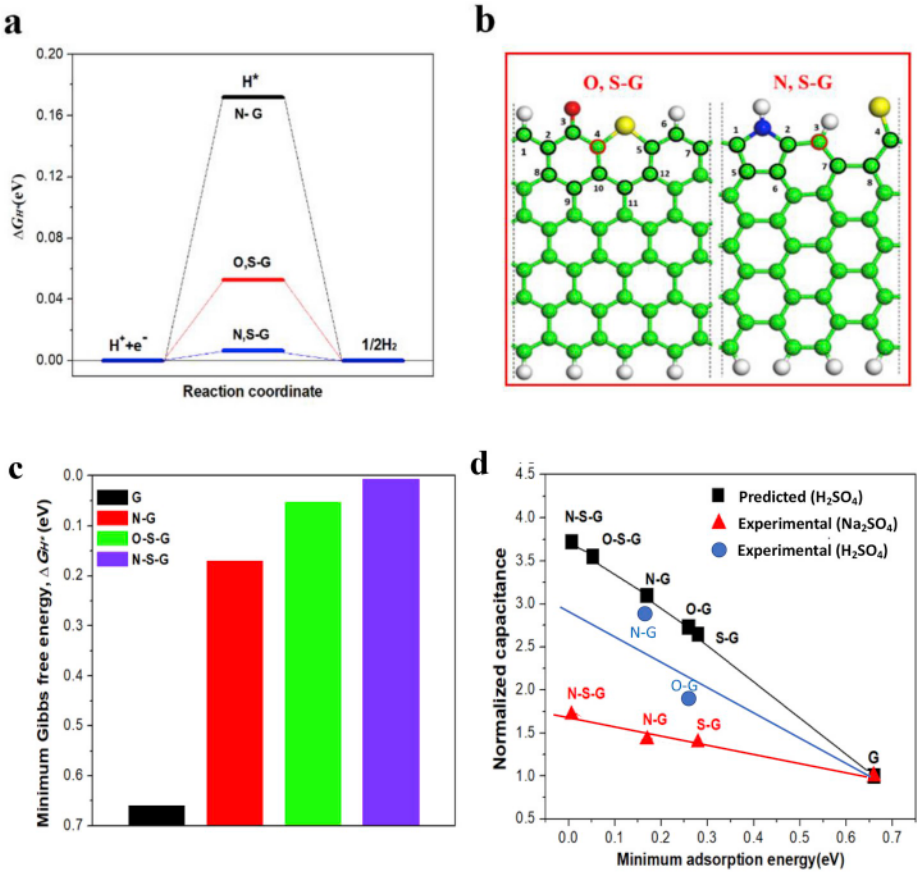

Fig. 5. Free energy diagram for double doped graphene models. a, the three-state free energy diagram for different types of double doped graphene. b, corresponding optimal doping structures for O, S- and N, S co-doping models. c, comparison between minimum hydrogen adsorption free energy for pristine, single-element doping, and double-element doping graphene. d, experimental and predicted capacitance, normalized by that of pure carbon, as a function of the minimum adsorption energy, $\Delta G_{H^*}^{min}$ for single and co-doped graphene structures in H_2SO_4 and Na_2SO_4 electrolytes.

2.4. Simultaneous improvement of both energy and power densities by doping

Generally, a pseudocapacitor usually has inferior energy density relative to batteries and poor power density compared with electric double layer capacitors (EDLCs). Currently there lacks an effective method to enhance these two properties simultaneously. This goal could be achieved through reducing the proton chemisorption energy barrier properly by heteroatom doping. We have calculated the energy and power densities of X-G electrode materials. For $0< \Delta G_{H^*}^{min} < eU < \Delta G_{H^*}^{max}$, the energy per unit charge storage site $E_{0/site}$ (unit, eV site^{-1}) and the area specific energy E_A (unit, J m^{-2}) (Support Information) can be calculated by

$$E_{0/site} = \frac{eUk_BT}{eU - \Delta G_{H^*}^{min}} ln\left[\frac{1}{2}\left(1 + e^{\frac{eU-\Delta G_{H^*}^{min}}{k_BT}}\right)\right] \quad (4)$$

where e is the charge of electron and U is the external potential. (See the details in Supplementary Information). As shown in Fig. 6a, the doping enhances the energy density because it reduces the ΔG_{H^*}. On the other hand, the doping lowers the threshold ($\Delta G_{H^*}^{min}/e$) of applied voltage in the charging. Only when $U \geq \Delta G_{H^*}^{min}/e$, can supercapacitors start to charge on the sites of the X-G, while the doping reduces the threshold voltage for charging because of lower $\Delta G_{H^*}^{min}$ compared with undoped graphene (Fig. 6a). More significantly, with the decrease of ΔG_{H^*}, energy density increases sharply, as shown in Fig. 6b. Once again, the significance of doping is demonstrated for the improvement of energy density.

Power density is defined as the change of energy per unit time. In general, the power density, or charging rate, is mainly governed by both conductivity of electrode, diffusion of protons in electrolytes, as well as the chemisorption rate of protons. For a given external condition such as ohmic resistance, H^+ diffusion, conductivity and charging potential in a supercapacitor, the chemisorption rate on the active sites (or chemical reaction rate) dominates the power density, which can be written as

$$P_{0/site} = k_0 \times \frac{eUk_BTln\left[\frac{1}{2}\left(1 + e^{\frac{eU-\Delta G_{H^*}^{min}}{k_BT}}\right)\right] - \frac{1}{2}\left(\Delta G_{H^*}^{min} - eU\right)^2}{\Delta G_{H^*}^{max} - \Delta G_{H^*}^{min} + k_BT\left(e^{\frac{\Delta G_{H^*}^{max}-eU}{k_BT}} + e^{\frac{\Delta G_{H^*}^{min}-eU}{k_BT}}\right)} \quad (5)$$

where k_0 and k_B are the rate constant and the Boltzmann constant, respectively (See the details in Supplementary Information). According to Equation (5), the charging rate not only depends on the intrinsic factor such as the doping structures, but also relies on the extrinsic factors including charging potential U, electrolytes and pH value. For a given charging system, the doping generally enhances the power density, depending on the types of the dopants, as illustrated in Fig. 6c. Overall, according to Equations (4) and (5), doping would reduce $\Delta G_{H^*}^{min}$, which would enhance both energy density and power density simultaneously for pseudocapacitors.

2.5. Strategies for designing carbon-based high-performance electrode materials

We have made DFT calculations to understand the origin of the X-G-based electrode materials and discovered an intrinsic descriptor that well describes the energy storage capacity of the materials. On the basis of the above results, both the energy and power densities are determined by intrinsic and extrinsic factors associated with active sites. As the

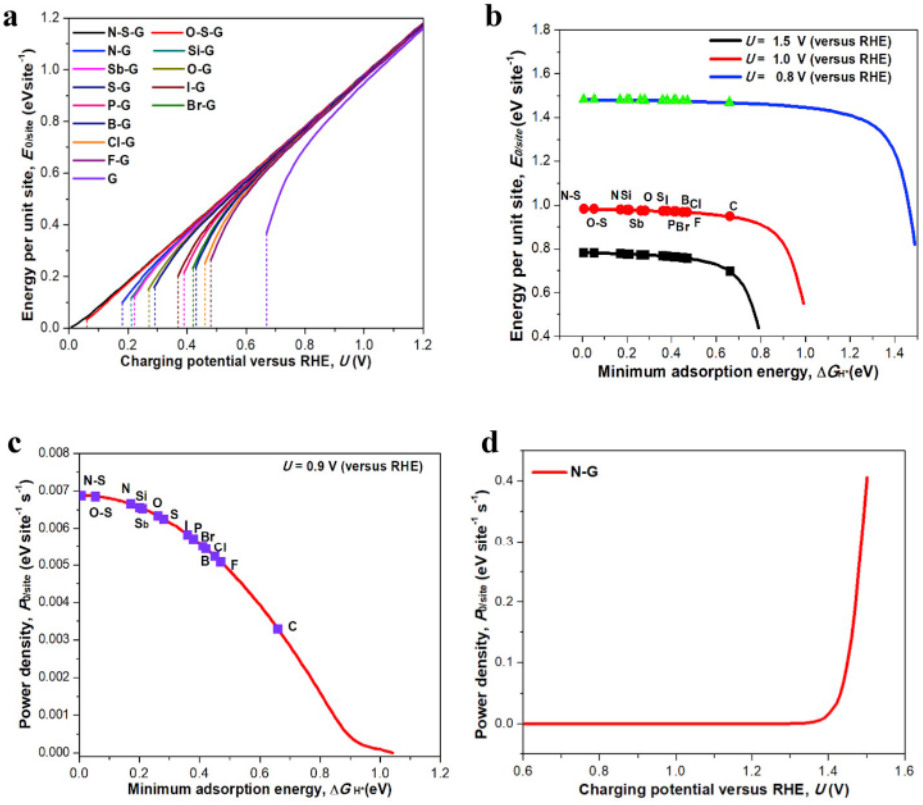

Fig. 6. Effect of the minimum adsorption energy and the charging potential on energy and power densities. a, energy per unit site versus charging potential U (versus RHE). **b**, energy per unit area versus minimum hydrogen adsorption energy $\Delta G_{H^*}^{min}$ at a given potential of U = 0.8, 1.0, and 1.5 V. **c**, power per unit site versus minimum hydrogen adsorption energy $\Delta G_{H^*}^{min}$ at a given potential of U = 0.9 V. **d**, power per unit site versus charging potential U at minimum hydrogen adsorption energy $\Delta G_{H^*}^{min}$ of 0.17 eV for N-doped graphene.

adsorption occurs only on the active sites, the charge storage activity of the X-G is directly related to the unit activity of the active sites (intrinsic factor), while the population of exposed active sites for a given electrode mass in energy devices is the extrinsic factor, which is related to the density of exposed active sites and the specific surface area (S_c). According to Equations (4) and (5), in addition to the intrinsic and extrinsic factors, environment factors (e.g., U and pH) also affect the proton adsorption of the electrodes. From above analysis, material design strategies can be established to achieve these predicted structures or functions by considering the intrinsic and extrinsic factors as well as the environmental factors. These strategies include as follows:

(i) *Create highly-effective active sites.* This material design strategy is to enhance the intrinsic activity of active centers (intrinsic factors). Doping using the p-block dopants with 0.5< Ø<2 and introducing more edges based on edge effect could significantly enhance the charge storage capacity. Co-doping, such as N, S and O, S co-doping, could further enhance the storage capacity due to the synergetic effect.

(ii) *Build 3D porous carbon or nanoarchitectures to expose more active sites.* This material design strategy is to populate more active sites on electrode surfaces (extrinsic factors). 3D porous carbon or nanoarchitecture electrodes could have a large specific-surface area to facilitate ion diffusion as well as increasing the number of exposed active sites.

(iii) *Control the capacitive environments.* According to Equations (4) and (5), the energy and power densities are strongly influenced by their environments and thus a strategy to facilitate them is to control catalytic environments (e.g., pH values, types of electrolytes, temperature, electric field). applying an electric field or changing pH values can directly change the interactions between adsorbates and electrode surfaces and consequently alter the thermodynamic and kinetic properties of the adsorption/desorption reactions.

3. Conclusion

The charging/discharging processes on heteroatom-doped graphene were analyzed with the DFT methods. The Gibbs free energy of adsorption, the capacitances, the energy and power densities were calculated to understand the origin of charge storage on the doped carbon surfaces. The results show that doping can significantly lower the Gibbs free energy of adsorption, and consequently enhance both energy and power densities. The co-doping can even further improve the charge storage capabilities due to the synergistic effect between the dopants. Introducing more graphene edges could also significantly enhance the charge storage capacity. A descriptor correlating charge storage capabilities with the doping structures was discovered, from which the optimal electrode structures could be predicted. Such a design principle provides a critical guidance for rational design of carbon-based electrodes for high-performance supercapacitors.

4. Methods

The adsorption of protons in acid electrolyte during the charging process of supercapacitors on various heteroatom-doped graphene surfaces were performed using the DFT methods with spin polarization, as implemented in the Vienna ab-initio Simulation Package (VASP) code [35]. The projector augmented wave (PAW) pseudo-potentials was used to describe nuclei-electron interactions, while the electronic exchange and correlation effects were modelled using the Perdew-Burke-Ernzerhof functional within the generalized gradient approximation (GGA) [36]. For plane wave basis set, a high kinetic energy cutoff of 400 eV was selected after testing several different cutoff energies. 10^{-5} eV was used as the convergence criterion of electronic structure iteration. For geometry optimization, convergence criterion for force of the system was set to be about 0.01 eV/Å. The K-points were set to be 4 × 4 × 1 and 4 × 1 × 1 for both graphene sheet models and graphene nanoribbon models, respectively. The choice of the k point

meshes and cutoff energy ensured that energies converged to about 1 meV per atom.

Three different groups of graphene models were developed to explore the adsorption effects of electrolyte ions in the charging process. The first group of graphene models are periodic on the *x*- and *y*-directions, respectively, consisting of 48 carbon atoms. The second group of models are armchair graphene nanoribbons consisting of 36 carbon atoms and 8 hydrogen atoms used to saturate dangling bonds at the edges of graphene. The third group of models are zigzag graphene nanoribbons comprising 48 carbon atoms and 8 hydrogen atoms. Both armchair and zigzag nanoribbons were constructed as a three-dimensional periodic structure with vacuum layers around 14 and 18 Å in the *y*- and *z*-directions, respectively, to avoid interaction between graphene slabs.

Declaration of competing interest

The authors declare that they have no known competing financial interests or personal relationships that could have appeared to influence the work reported in this paper.

CRediT authorship contribution statement

Zhenghang Zhao: Conceptualization, Methodology.

Acknowledgements

This work is supported financially by the U.S. National Science Foundation (1662288), National Natural Science Foundation of China (51704243), the Fundamental Research Funds for the Central Universities (3102019ZD0402) and Innovation Foundation for Doctor Dissertation of Northwestern Polytechnical University, China (CX201943).

Appendix A. Supplementary data

Supplementary data to this article can be found online at https://doi.org/10.1016/j.nanoen.2020.104666.

References

[1] C. Zhan, D.E. Jiang, J. Phys. Chem. Lett. 7 (2016) 789.
[2] Y. Zhu, S. Murali, M.D. Stoller, K.J. Ganesh, W. Cai, P.J. Ferreira, A. Pirkle, R. M. Wallace, K.A. Cychosz, M. Thommes, D. Su, E.A. Stach, R.S. Ruoff, Science 332 (2011) 1537.
[3] M.F. El-Kady, V. Strong, S. Dubin, R.B. Kaner, Science 335 (2012) 1326.
[4] Y. Xu, Z. Lin, X. Huang, Y. Liu, Y. Huang, X. Duan, ACS Nano 7 (2013) 4042.
[5] C. Huang, J. Zhang, N.P. Young, H.J. Snaith, P.S. Grant, Sci. Rep. 6 (2016) 25684.
[6] C. Prehal1, C. Koczwara, N. Jäckel, A. Schreiber, M. Burian, H. Amenitsch, M. A. Hartmann, V. Presser, O. Paris, Nat. energy 2 (2017) 16215.
[7] N. Choudhary, C. Li, J. Moore, N. Nagaiah, L. Zhai, Y. Jung, J. Thomas, Adv. Mater. 29 (2017) 1605336.
[8] D. Sheberla, J.C. Bachman, J.S. Elias, C.J. Sun, Y.S. Horn, M. Dinca, Nat. Mater. 16 (2017) 220.
[9] M. Boota, B. Anasori, C. Voigt, M.Q. Zhao, M.W. Barsoum, Y. Gogotsi, Adv. Mater. 10 (2015) 1002.
[10] X.Y. Lang, A. Hirata, T. Fujita, M.W. Chen, Nat. Nanotechnol. 6 (2011) 232.
[11] N.A. Kyeremateng, T. Brousse, D. Pech, Nat. Nanotechnol. 12 (2017) 7.
[12] M.R. Lukatskaya, S. Kota, Z.F. Lin, M.Q. Zhao, N. Shpigel, M.D. Levi, J. Halim, P. L. Taberna, M.W. Barsoum, P. Simon, Y. Gogotsi, Nat. energy 2 (2017) 16215.
[13] Z.H. Zhao, M.T. Li, L.P. Zhang, L.M. Dai, Z.H. Xia, Adv. Mater. 27 (2015) 6834.
[14] J.T. Zhang, Z.H. Zhao, Z.H. Xia, L.M. Dai, Nat. Nanotechnol. 10 (2015) 444.
[15] Y. Gao, Y.Y. Wan, B.Q. Wei, Z.H. Xia, Adv. Funct. Mater. 1706721 (2018) 1.
[16] X.F. Jiang, X.B. Wang, P.C. Dai, X. Li, Q.H. Weng, X. Wang, D.M. Tang, J. Tang, Y. Bando, D. Golberg, Nano Energy 16 (2015) 81.
[17] X.L. Su, J.R. Chen, G.P. Zheng, J.H. Yang, X.X. Guan, P. Liu, X.C. Zheng, Appl. Surf. Sci. 436 (2018) 327.
[18] D. Pech, M. Brunet, H. Durou, P.H. Huang, V. Mochalin, Y. Gogotsi, P.L. Taberna, P. Simon, Nat. Nanotechnol. 5 (2010) 651.
[19] D.S. Yu, K. Goh, H. Wang, L. Wei, W.C. Jiang, Q. Zhang, L.M. Dai, Y. Chen, Nat. Nanotechnol. 9 (2014) 555.
[20] P. Chen, J.J. Yang, S.S. Li, Z. Wang, T.Y. Xiao, Y.H. Qian, S.H. Yun, Nano Energy 2 (2013) 249.
[21] J.W. Han, L.L. Zhang, S. Lee, J. Oh, K.S. Lee, J.R. Potts, J.Y. Ji, X. Zhao, R.S. Ruoff, S. Park, ACS Nano 7 (2013) 19.
[22] J.N. Yi, Y. Qing, C.T. Wu, Y.X. Zeng, Y.Q. Wu, X.H. Lu, Y.X. Tong, J. Power Sources 351 (2017) 130.
[23] Y.Y. Wen, B. Wang, C.C. Huang, L.Z. Wang, D.H. Jurcakova, Chem. Eur J. 20 (2014) 1.
[24] S. Gong, Q. Wang, J. Phys. Chem. C 121 (2017) 24418.
[25] F. Yu, Z.C. Liu, R.W. Zhou, D.M. Tan, H.X. Wang, F.X. Wang, J. Mater. Chem. A (2013) 1, 00.
[26] J.L. Xia, F. Chen, J.H. Li, N.J. Tao, Nat. Nanotechnol. 4 (2009) 505.
[27] D.W. Wang, F. Li, Z.G. Chen, G.Q. Lu, H.M. Cheng, Chem. Mater. 20 (2008) 7195.
[28] P. Karthika, N. Rajalakshmi, K.S. Dhathathreyan, J. Nanosci. Nanotechnol. 12 (2012) 1.
[29] X. Yu, Y.B. Kang, H.S. Park, Carbon 101 (2016) 49.
[30] Y.S. Yun, H.H. Park, H.J. Jin, Materials 5 (2012) 1258.
[31] Y.J. Oh, J.J. Yoo, Y.I. Kim, J.K. Yoon, H.N. Yoon, J.H. Kima, S.B. Park, Electrochim. Acta 116 (2014) 118.
[32] K. Kakaei, M. Hamidi, S. Husseindoost, J. Colloid Interface Sci. 479 (2016) 121.
[33] K. Gopalsamy, J. Balamurugan, T.D. Thanh, N.H. Kim, J.H. Lee, Chem. Eng. J. 312 (2017) 180.
[34] S. Bag, B. Mondal, A.K. Das, C.R. Raj, Electrochim. Acta 163 (2015) 16.
[35] G. Kresse, J. Furthmüller, Phys. Rev. B: Condens. Matter Mater. Phys. 54 (1996) 11169.
[36] I.V. Solvyev, P.H. Dederichs, V.I. Anisimov, Phys.Rev. B 50 (1994) 16861.